Statistical mechanics of semiflexible ribbon polymers

Ramin Golestanian [1,2,3] and Tanniemola B. Liverpool[1,4,*]
[1]*Max-Planck-Institut für Polymerforschung, D-55021 Mainz, Germany*
[2]*Institute for Advanced Studies in Basic Sciences, Zanjan 45195-159, Iran*
[3]*Institute for Theoretical Physics, University of California, Santa Barbara, California 93106-4030*
[4]*Physico-Chimie Théorique, ESA CNRS 7083, ESPCI, 75231 Paris Cedex 05, France*
(Received 1 November 1999; revised manuscript received 11 May 2000)

The statistical mechanics of a ribbon polymer made up of two semiflexible chains is studied using both analytical techniques and simulation. The system is found to have a crossover transition at some finite temperature, from one type of short-range order to a fundamentally different sort of short-range order. In the high temperature regime, the two-point correlation functions of the object are identical to wormlike chains, while in the low temperature regime they are different due to a twist structure. The crossover happens when the persistence length of individual strands becomes comparable to the thickness of the ribbon. In the low temperature regime, the ribbon is observed to have a ''kink-rod'' structure with a mutual exclusion of twist and bend in contrast to smooth wormlike chain behavior. This is due to its anisotropic rigidity and corresponds to an *infinitely* strong twist-bend coupling. The double-stranded polymer is also studied in a confined geometry. It is shown that when the polymer is restricted in a particular direction to a size less than the bare persistence length of the individual strands, it develops zigzag conformations which are indicated by an oscillatory tangent-tangent correlation function in the direction of confinement. Increasing the separation of the confining plates leads to a crossover to the free behavior, which takes place at separations close to the bare persistence length. These results are expected to be relevant for experiments that involve complexation of two or more stiff or semiflexible polymers.

PACS number(s): 87.15.By, 36.20.Ey, 61.25.Hq

I. INTRODUCTION AND SUMMARY

There has been a lot of recent interest in physical properties of biopolymers, ranging from elasticity of biopolymer networks and its use in the prediction of mechanical properties of cells to direct visualization of single-chain properties. Examples of important biological macromolecules whose physical properties have been recently studied are actin, a double-stranded semiflexible protein polymer which forms an integral part of the cytoskeleton (mechanical structure) of eukaryotic (e.g., fungi, plants, animals) cells; microtubules, multistranded rigid and dynamic protein polymers which form one of the main components of the cytoskeleton of eukaryotic cells and play an important part in their organization; DNA, which carries the genetic code of all living organisms [1].

Since many of the processes involved in cell function (e.g., DNA replication in cell division) require major structural changes of these biopolymers [2], there is a need for more microscopic but still analytically tractable models of such polymers that go beyond the simple picture of such molecules as homogeneous elastic rods [3]. Motivated by this, we study such a microscopic model, specifically looking for qualitative differences between the behavior of such molecules and simple wormlike chains [4]. In addition, most analyses of the wormlike chain models of polymers have focused on ground state properties (long chains) or bulk quantities [5]. It is interesting to look at the effects of fluctuations, spatial correlations, *and* finite size on these systems.

A double-stranded semiflexible polymer chain is the basic structure of many biopolymers. Examples of double-stranded biopolymers are DNA and proteins such as actin. The model most used in the study of biopolymers is that of the wormlike chain [4] in which the polymer flexibility (structure) is determined by a single length, the persistence length ℓ_p, which measures the tangent-tangent correlations. For example, DNA has a persistence length $\ell_p \approx 50$ nm while for actin $\ell_p \approx 17$ μm. These biopolymers are known to have a complex ''twisted'' structure. The multistranded nature of these polymers is also not taken into account in a simple wormlike chain model. It is not clear if such a fine structure will have an effect on the global properties of these objects. A possible effect of such fine structure is what we attempt to study in this article. Our model is, in a sense, microscopic because the interaction between the bend and twist degrees of freedom is a *result*. This is fundamentally different from previous approaches [3], which try to include the twist degrees of freedom by adding extra terms to the free energy.

In a previous report [7] we studied a version of the railway track model of Everaers-Bundschuh-Kremer [6] for a double-stranded semiflexible polymer, embedded in a d-dimensional space for arbitrary d. The main purpose of this article is to present a detailed description of our theoretical and numerical calculations and in addition we present some results on the effect of confinement on the statistical mechanics of the ribbon polymer [8]. Excluded volume and electrostatic interactions have been ignored throughout.

We find that the system has qualitatively different properties in the low temperature and high temperature regimes, in contrast to what one might naively expect from an inher-

*Present address: Blackett Laboratory, Imperial College, Prince Consort Road, London SW2 2BZ, United Kingdom.

ently one-dimensional system with local interactions and constraints. The tangent-tangent correlation function decays exponentially in the whole range of temperatures with a ''tangent-persistence length'' ℓ_{TP} that has a very slow temperature dependence, and whose scale is determined by the (bare) persistence length of a single strand $\ell_p=\kappa/k_BT$ (κ is the bending stiffness of a single strand). Note that it is independent of a, the separation of the two strands, which is the other relevant length scale in the problem. However, the correlation function of the bond-director field, defined as a vector that determines the separation and coupling of the two strands of the combined polymer system, has different behavior below and above the temperature $T_\times \simeq 4.27\kappa/dk_Ba$. While it decays purely exponentially for $T>T_\times$, there are additional oscillatory modulations for $T<T_\times$. The related ''bond-persistence length'' ℓ_{BP} does not change appreciably at high temperatures, where its scale is again set by ℓ_p alone. In the low temperature phase, however, ℓ_{BP} does show a temperature dependence. In particular, $\ell_{\mathrm{BP}}\sim\ell_p^{1/3}a^{2/3}\propto T^{-1/3}$ for $T\sim 0$, while $\ell_{\mathrm{BP}}\sim\ell_p$ for $T\sim T_\times$. Similarly, the ''pitch'' H, defined as the period of oscillations in the low temperature regime, changes drastically with temperature, ranging from $H\sim\ell_{\mathrm{BP}}\sim\ell_p^{1/3}a^{2/3}$ near $T=0$ to $H\sim 0$ near $T=T_\times$. At $T=0$ we regain a flat ribbon that has true long-range order in both the tangent and bond-director fields. The ribbon is essentially a rigid rod. As we approach $T=0$, the persistence lengths and the pitch diverge with the scaling $H\sim\ell_{\mathrm{BP}}\sim\ell_{\mathrm{TP}}^{1/3}$.

The spontaneous appearance of a short-range twist structure may be understood in the language of the homogeneous rod models [3] as a local twist-bend coupling, which is observed up to a screening length ℓ_{BP} that lies between a and ℓ_p. We find that the anisotropy in the rigidity of a ribbon results in a ''kink-rod'' structure, in which the ribbon is at every point along its contour either twisted and unbent (rod) or bent and untwisted (kink). This inhomogeneous behavior is in sharp contrast with uniform wormlike chain behavior, and can be interpreted as an infinitely strong twist-bend coupling. This structure is, however, screened (i.e., decays to zero) on long length scales due to the fact that the ribbon is a one-dimensional system with short-range interactions. The short-range twist order and the kink-rod structure will naturally disappear when $a\sim\ell_p$ corresponding to the temperature $T_\times$. We also observe a twist-stretch coupling.

We also study the effects of confinement on the double-stranded polymer. We enforce the confinement to a box of size R as an additional constraint. For $R\gg\ell_p$, we recover the behavior of free double-stranded semiflexible polymers [7]. In particular, the tangent-tangent correlation has a purely exponential decay with a characteristic length scale of order ℓ_p, while the bond-director field develops a crossover to a phase with oscillatory correlations. As R is decreased, there is a crossover to a phase with oscillatory tangent-tangent correlations about $R\sim\ell_p$. For $R\ll\ell_p$, we find that both the persistence length in the perpendicular direction $\ell_\perp$ and the characteristic oscillation length λ scale as $(\ell_pR^2)^{1/3}$, which is considerably smaller than ℓ_p. The same crossover in the bond-director field also persists in this limit, and, in particular, there is a regime in which both the tangent and the bond-director correlations are oscillatory.

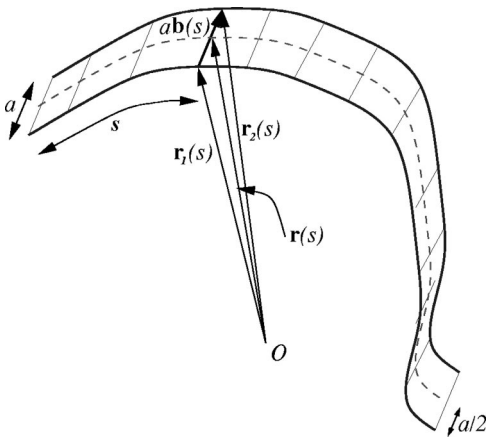

FIG. 1. The schematic of the double-stranded semiflexible polymer of two chains separated by a distance a. Note the bond-director field $\mathbf{b}(s)$.

We introduce and define our model in Sec. II, and then describe a mean field approach in Sec. III that can be used to obtain closed form expressions for various correlation functions. In Sec. IV we discuss a physical argument for the results we obtain using a plaquette model. In Sec. V we describe some extensive molecular dynamics/Monte Carlo simulations, which we use to calculate the correlation functions, and compare them with the mean field results of Sec. III. We discuss the thermal kink-rod structure of stiff ribbons in Sec. VI, and the effects of confinement on the conformations of ribbon polymers in Sec. VII. Finally, Sec. VIII summarizes our results and the limitations of our approach.

II. RAILWAY TRACK MODEL

To study the effect of a double structure on semiflexible polymers, we consider a version of the railway track model of Everaers-Bundschuh-Kremer [6]. In our approach, we are able to consider polymers embedded in a d-dimensional space for arbitrary d. The system is composed of two semiflexible chains, each with rigidity κ, whose embeddings in d-dimensional space are defined by $\mathbf{r}_1(s)$ and $\mathbf{r}_2(s)$. The Hamiltonian of the system can be written as the sum of the Hamiltonians of two wormlike chains:

$$\mathcal{H}=\frac{\kappa}{2}\int ds\left[\left(\frac{d^2\mathbf{r}_1(s)}{ds^2}\right)^2+\left(\frac{d^2\mathbf{r}_2(s)}{ds^2}\right)^2\right]. \tag{1}$$

We assume that the individual strands (that make up the double-stranded polymer) are inextensible: $(d\mathbf{r}_1/ds)^2=(d\mathbf{r}_2/ds)^2=1$. The ribbon structure is then enforced by having $\mathbf{r}_2(s')$ separated from $\mathbf{r}_1(s)$ by a distance a, i.e., $\mathbf{r}_2(s')=\mathbf{r}_1(s)+a\mathbf{b}(s)$, where $|s-s'|$ can be nonzero but is small. We have defined a bond-director field $\mathbf{b}(s)$, which is a unit vector perpendicular to both strands (see Fig. 1). The chains are assumed to have permanent bonds (such as hydrogen bonds) that are strong enough to keep the distance between the two strands constant. In Ref. [6], it is argued that the relevant constraint on the system would then require that the arclength mismatch between the two strands in a bent configuration should be very small. We can calculate the arclength mismatch for the bent configuration as Δs

$=|\mathbf{r}_2(s)-\mathbf{r}_1(s)+a\mathbf{b}(s)|$, where a is the separation of the strands. We impose the constraint as a hard one, namely, we set $\Delta s=0$ as opposed to Ref. [6]. Physically this means we do not allow bends in the plane of the ribbon. These bends are not important in $d>2$ because as we shall see the lower length scale will be set by the ''pitch,'' which will make the in-plane fluctuations of the ribbon irrelevant [6].

We can argue that the simplifying assumption does not change the behavior of the system. If we impose a soft constraint as in Ref. [6] using an energy term like $(k/2)\int(\Delta s)^2$, we can see that the length $l=(\kappa/ka^2)^{1/2}$ determines two different regimes; the interesting one being $L\gg l$ (L is the length of the chains). Hence, our hard constraint in fact only restricts us to the case of interest.

We implement the constraint $\Delta s=0$ by introducing the ''mid-curve'' $\mathbf{r}(s)$:

$$\mathbf{r}_1(s)=\mathbf{r}(s)+\frac{a}{2}\mathbf{b},$$
$$\mathbf{r}_2(s)=\mathbf{r}(s)-\frac{a}{2}\mathbf{b}. \tag{2}$$

In terms of the tangent to the mid-curve $\mathbf{t}=d\mathbf{r}/ds$, which we call the tangent-director field, and the bond-director $\mathbf{b}$, the Hamiltonian of the system can now be written as

$$\mathcal{H}=\frac{\kappa}{2}\int ds\left[2\left(\frac{d\mathbf{t}(s)}{ds}\right)^2+\frac{a^2}{2}\left(\frac{d^2\mathbf{b}(s)}{ds^2}\right)^2\right], \tag{3}$$

subject to the exact (local) constraints

$$\left(\mathbf{t}\pm\frac{a}{2}\frac{d\mathbf{b}}{ds}\right)^2=1,\quad \mathbf{b}^2=1,$$
$$\left(\mathbf{t}\pm\frac{a}{2}\frac{d\mathbf{b}}{ds}\right)\cdot\mathbf{b}=0. \tag{4}$$

For a weakly bent ribbon, the Hamiltonian in Eq. (3) can be conveniently thought of as having two major contributions: a bending energy $\mathcal{H}_b$ (the first term), and a twisting energy $\mathcal{H}_t$ (the second term).

III. MEAN FIELD THEORY: FREE CHAINS

It is well known that the statistical mechanics of semiflexible chains are difficult due to the constraint of inextensibility. Various approximation methods have been devised to tackle the problem. A successful scheme that somehow manages to capture the crucial features of the problem is to impose global (average) constraints rather than local (exact) ones [9–13]. This approximation is known to be good for calculating the average end-to-end length. It can be used for the probability distribution of the end-to-end length only if the persistence length is much less than the chain length so that the chain conformation can be considered isotropic. We can get good insight into the approximation scheme by considering the fact that it corresponds to a saddle-point evaluation of the integrals over the Lagrange multipliers, which are introduced to implement the constraints [12,13]. In this sense, it is known to be a ''mean field'' approximation in spirit. One can then go further by considering the effect of fluctuations on this mean field result. The power of this approach is that one can easily calculate quantities that turn out to be very difficult if the constraints are required to hold exactly [5].

To study the effect of fluctuations, we have performed a systematic $1/d$ expansion (sketched in the Appendix) [14]. We see that no divergent behavior appears when we calculate the diagrams of the two-point correlation functions. This means that the mean field behavior of these functions, at least, will not change due to fluctuations, although it does not preclude differences in higher order correlation functions.

With the above discussion as justification, we apply the same approximation scheme to our problem as defined in Sec. II: The local constraints in Eq. (4) are relaxed to global ones. This can be done by adding the corresponding ''mass terms'' to the Hamiltonian,

$$\frac{\mathcal{H}_m}{k_BT}=\int ds\left[\frac{b}{\ell_p}\left(\mathbf{t}-\frac{a}{2}\frac{d\mathbf{b}}{ds}\right)^2+\frac{b}{\ell_p}\left(\mathbf{t}+\frac{a}{2}\frac{d\mathbf{b}}{ds}\right)^2+\frac{ca^2}{4\ell_p^3}\mathbf{b}^2\right.$$
$$\left.+\frac{e}{\ell_p}\left(\mathbf{t}-\frac{a}{2}\frac{d\mathbf{b}}{ds}\right)\cdot\mathbf{b}+\frac{e}{\ell_p}\left(\mathbf{t}+\frac{a}{2}\frac{d\mathbf{b}}{ds}\right)\cdot\mathbf{b}\right], \tag{5}$$

where b, c, and e are dimensionless constants. The partition function is then given by

$$Z[\mathbf{J},\mathbf{K}]=\int\mathcal{D}\mathbf{t}(s)\mathcal{D}\mathbf{b}(s)\exp\left(-\frac{\mathcal{H}+\mathcal{H}_m}{k_BT}\right.$$
$$\left.+\int ds[\mathbf{J}(s)\cdot\mathbf{t}(s)+\mathbf{K}(s)\cdot\mathbf{b}(s)]\right). \tag{6}$$

We next determine the constants self-consistently by demanding the constraints of Eq. (4) to hold on average, where the thermal average is calculated by using the total Hamiltonian $\mathcal{H}+\mathcal{H}_m$. Note that in choosing the above form we have implemented the ''label symmetry'' of the chains, namely, that there is no difference between two chains. It is convenient to take the limit of an infinitely long chain and perform the functional integrals in momentum space. The Fourier transforms are defined as $\tilde{\mathbf{A}}(q)=\int ds\,\exp(iqs)\mathbf{A}(s)$. We have

$$Z[\tilde{\mathbf{J}},\tilde{\mathbf{K}}]=\int\mathcal{D}\tilde{\mathbf{t}}(q)\mathcal{D}\tilde{\mathbf{b}}(q)\exp\left[-\frac{1}{2}\int\frac{dq}{2\pi}\right.$$
$$\times[\tilde{\mathbf{t}}(-q),\tilde{\mathbf{b}}(-q)]\cdot\overline{\mathbf{M}}(q)\cdot\begin{pmatrix}\tilde{\mathbf{t}}(q)\\ \tilde{\mathbf{b}}(q)\end{pmatrix}$$
$$\left.+\int\frac{dq}{2\pi}(\tilde{\mathbf{J}}\cdot\tilde{\mathbf{t}}+\tilde{\mathbf{K}}\cdot\tilde{\mathbf{b}})\right]. \tag{7}$$

The Gaussian integration can then be easily performed. It yields

$$Z[\tilde{\mathbf{J}},\tilde{\mathbf{K}}]=\exp\left(\frac{1}{2}\int\frac{dq}{2\pi}\right.$$

$$\left.\times[\tilde{\mathbf{J}}(-q),\tilde{\mathbf{K}}(-q)]\cdot\overline{\mathbf{M}}^{-1}(q)\cdot\begin{pmatrix}\tilde{\mathbf{J}}(q)\\ \tilde{\mathbf{K}}(q)\end{pmatrix}\right), \quad (8)$$

where

$$\overline{\mathbf{M}}(q)=\begin{bmatrix}2\ell_p q^2+4b/\ell_p & 2e/\ell_p\\ 2e/\ell_p & \ell_p a^2q^4/2+ba^2q^2/\ell_p+ca^2/\ell_p^3\end{bmatrix}. \quad (9)$$

The averages are easily obtained from Z, for example,

$$\langle\tilde{t}_i(q)\cdot\tilde{b}_j(q')\rangle=\frac{\delta^2\ln Z}{\delta\tilde{J}_i(q)\,\delta\tilde{K}_j(q')}.$$

The next step is to demand self-consistently that

$$\langle\mathbf{b}(s)^2\rangle=1,$$

$$\left\langle\left(\mathbf{t}(s)\pm\frac{a}{2}\frac{d\mathbf{b}(s)}{ds}\right)^2\right\rangle=1, \quad (10)$$

$$\left\langle\left(\mathbf{t}(s)\pm\frac{a}{2}\frac{d\mathbf{b}(s)}{ds}\right)\cdot\mathbf{b}(s)\right\rangle=0.$$

The self-consistency leads to the following set of equations for the constants b, c, and e:

$$\frac{1}{4\sqrt{2b}}+\frac{a^2\sqrt{c}}{4d\ell_p^2}=\frac{1}{d},$$

$$c(b+\sqrt{c})=\frac{d^2\ell_p^4}{2a^4}, \quad (11)$$

$$e=0.$$

The above equations, which are nonlinear and difficult to solve exactly, determine the behavior of b and c as a function of $u=a/\ell_p$. We have solved them numerically in $d=3$ and the solutions are given in Fig. 2. One can solve Eq. (11) analytically in two limiting cases. For $u\ll 1$ we find $b=d^2/32$ and $c=(d/\sqrt{2})^{4/3}u^{-8/3}$, whereas for $u\gg 1$ we find $b=d^2/8$ and $c=4/u^4$. In Fig. 2, the behavior of b and c is plotted as a function of u. Note that u is proportional to T and can be viewed as a measure of temperature.

We can then calculate the correlation functions. For the tangent-tangent correlation one obtains

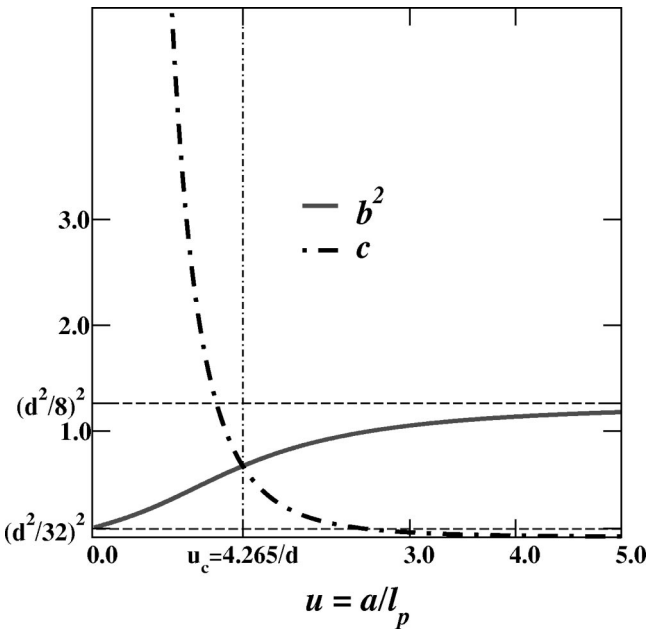

FIG. 2. The solution of the self-consistent equations for the constants b and c as functions of $u=a/\ell_p$ in $d=3$. The value $u_c\simeq 4.27/d$ corresponds to the transition point.

$$\langle\mathbf{t}(s)\cdot\mathbf{t}(0)\rangle=\frac{d}{4\sqrt{2b}}\exp\left(-\sqrt{2b}\,\frac{s}{\ell_p}\right), \quad (12)$$

whereas for the bond-director field one obtains

$$\langle\mathbf{b}(s)\cdot\mathbf{b}(0)\rangle=\frac{d\ell_p^2}{2a^2\sqrt{b^2-c}}\left[\frac{\exp[-(b-\sqrt{b^2-c})^{1/2}(s/\ell_p)]}{(b-\sqrt{b^2-c})^{1/2}}\right.$$

$$\left.-\frac{\exp[-(b+\sqrt{b^2-c})^{1/2}(s/\ell_p)]}{(b+\sqrt{b^2-c})^{1/2}}\right]. \quad (13)$$

The tangent-tangent correlation [Eq. (12)] is exactly what we obtain for a single wormlike chain, and implies uniform behavior for all temperatures. Equation (13), on the other hand, indicates a change of behavior at $b^2=c$ for the bond-director correlation. The correlation is overdamped for $b^2>c$ (high temperatures), while it is underdamped (oscillatory) for $b^2<c$ (low temperatures). The interesting point $b^2=c$ happens for $u_c=16/(1+\sqrt{2})^{3/2}d\simeq 4.27/d$, which leads to the value for $T_\times$ quoted above (see Fig. 2). We also find a divergence in the specific heat $C_V=\partial^2F/\partial T^2$ where $F=-k_BT\ln Z$ at $T_\times$. It should be noted that it is not a thermodynamic phase transition in the sense of long-range ordering and broken symmetry. It is a crossover that appears due to competing effects, and the transition is from a state with some short-range order to a state with a different short-range order. Similar phenomena have been observed in Ising-like spin systems with competing interactions [15] and the crossover (transition) point corresponds to a type of ''Lifshitz point'' for a one-dimensional (1D) system.

It is interesting to study the bond-director correlation in the limiting case $b^2\ll c$, which corresponds to relatively low temperatures. Using the asymptotic forms for b and c, one obtains

$$\langle \mathbf{b}(s)\cdot\mathbf{b}(0)\rangle = \sqrt{2}\exp\left[-\left(\frac{d}{4\ell_p a^2}\right)^{1/3} s\right] \times \sin\left[\left(\frac{d}{4\ell_p a^2}\right)^{1/3} s+\frac{\pi}{4}\right] \tag{14}$$

for very low temperatures. From the above expressions for the correlation functions, one can read off the persistence lengths $\ell_{\mathrm{TP}}\sim\ell_p$ and $\ell_{\mathrm{BP}}\sim(\ell_p a^2)^{1/3}$, and the pitch $H\sim(\ell_p a^2)^{1/3}$.

From the tangent-tangent correlation function, we can calculate the end-to-end distance. It yields

$$\langle[\mathbf{r}(s)-\mathbf{r}(0)]^2\rangle = \int_0^s\int_0^s ds_1 ds_2\langle\mathbf{t}(s_1)\cdot\mathbf{t}(s_2)\rangle = \frac{d\ell_p}{4b}\left(s-\frac{\ell_p}{\sqrt{2b}}(1-e^{-\sqrt{2b}s/\ell_p})\right), \tag{15}$$

which is similar to wormlike chains. It interpolates between the limiting behaviors of random walks $[\sim(d\ell_p/4b)s]$ for $s\gg\ell_p$ and rods $[\sim(d/4\sqrt{2b})s^2]$ for $s\ll\ell_p$. However, it is interesting to note that there is a shrinking in the length of the rod by a factor of $(d/4\sqrt{2b})^{1/2}$, which varies smoothly from 1 at $a\ll\ell_p$ to $1/\sqrt{2}$ at $a\gg\ell_p$. This implies that a polymer made up of two inextensible strands is always ''slightly extensible'' at any finite temperature, due to the presence of twist fluctuations. This is exactly the twist-stretch coupling studied by various authors using homogenous elastic rod models [3]. Note that in our model this coupling is a *result*, as opposed to the elastic rod models in which it must be added by hand. A microscopic model proposed by O'Hern *et al.* [16], which describes DNA as a stack of plates, also predicts a twist-stretch coupling.

A simple scaling argument can account for ℓ_{TP} and ℓ_{BP} in the low temperature regime. Consider applying a uniform bend of radius of curvature λ to a section of ribbon of length λ without twisting it. The corresponding bending energy (calculated using $\mathcal{H}_b$) is given by $E_b\sim k_BT\ell_p/\lambda$. We can then estimate ℓ_{TP} by finding the length λ for which the bending energy E_b becomes comparable to k_BT. Similarly, applying a uniform twist per length $2\pi/\lambda$ to a section of the ribbon of length λ without bending will cost a twist energy $E_t=k_BT\ell_p a^2/\lambda^3$ (calculated using $\mathcal{H}_t$). The wavelength λ at which the twist energy E_t becomes comparable to k_BT gives ℓ_{BP}.

IV. PLAQUETTE MODEL AND COMPETITION

The nature of competition in our double-stranded polymer system can be understood using a plaquette model. We can coarse-grain the ribbon to a length scale (ℓ) where we can consider it to be made up of plaquettes which are joined up to form a ribbon (see Fig. 3). We can then define effective coarse-grained bond $\hat{\mathbf{B}}_i$ and tangent $\hat{\mathbf{T}}_i$ director fields for each plaquette.

The energy expression corresponding to bends comes from the product of the tangent directors of the neighboring plaquettes:

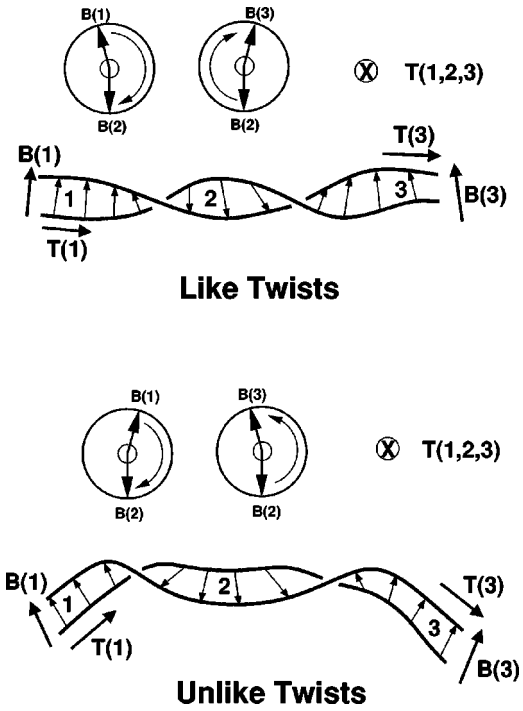

FIG. 3. Coarse-grained model—like and unlike twists meeting. The bond vector **B** is rotating about the tangent vector in the same direction for like twists and the opposite direction for unlike twists.

$$\beta\mathcal{H}_b = -\frac{\ell_p}{\ell}\sum_i \hat{\mathbf{T}}_i\cdot\hat{\mathbf{T}}_{i+1}. \tag{16}$$

In a spin analogy, this corresponds to a classical Heisenberg ferromagnet in 1D, and has no competition .

If we choose $\ell\ll\ell_p$ in the coarse-graining process, we can safely assume that the ribbon is rodlike (we freeze out the bending modes) and that it has only twist fluctuations. We may then write $\mathbf{b}(s)=\hat{\mathbf{e}}_1\cos\theta(s)+\hat{\mathbf{e}}_2\sin\theta(s)$ where the (fixed) unit vectors $\hat{\mathbf{e}}_i\,(i=1,2)$ span the plane perpendicular to the rod. Rewriting Eq. (3) in terms of $\theta(s)$ and implementing the constraints, we obtain

$$\beta\mathcal{H}=\frac{\ell_p a^2}{4}\int ds\left(|\partial_s^2\theta|^2+|\partial_s\theta|^4+\frac{a^2|\partial_s^2\theta|^2|\partial_s\theta|^2}{4-a^2|\partial_s\theta|^2}\right), \tag{17}$$

subject to the constraint $|\partial_s\theta(s)|<2/a$. Note that the lowest order contribution to the twist potential starts from a quartic term.

We can now expand the nonlinear term in the above Hamiltonian and perform the coarse graining, in the framework of a perturbation theory, by integrating out the modes between $1/\ell$ and $1/a$ in the momentum shell. We can then determine the form of the coarse-grained Hamiltonian and calculate the renormalized coupling constants. We keep only terms up to second (Gaussian) order, which is a good approximation for $\ell<(\ell_p a^2)^{1/3}$, and obtain

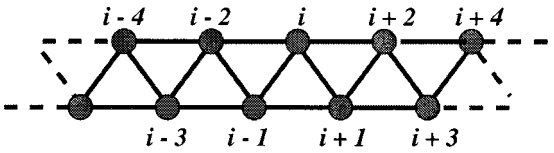

FIG. 4. The schematic of the double-strand model used in the simulation.

$$\beta\mathcal{H}_t = -J_1\sum_i \hat{\mathbf{B}}_i\cdot\hat{\mathbf{B}}_{i+1} - J_2\sum_i \hat{\mathbf{B}}_i\cdot\hat{\mathbf{B}}_{i+2} \tag{18}$$

where

$$J_1 = c_0 + c_1\frac{\ell_p a^2}{\ell^3} \quad \text{and} \quad J_2 = -c_2\frac{\ell_p a^2}{\ell^3},$$

where c_i $(i=0,\ldots,2)$ are constants of order unity. In contrast to the bending energy, the effective twist energy is frustrated due to the opposite signs of J_1 and J_2 [15]. In the spin analogy, this would correspond to a model with next nearest neighbor competing interactions similar to the so-called axial next nearest neighbor interaction (ANNNI) model, which develops oscillations for certain values of the ratio $-J_2/J_1$ (of order 1) [15]. This corresponds to $\ell\sim(\ell_p a^2)^{1/3}$, and we can thus account for the pitch $H\sim(\ell_p a^2)^{1/3}$.

The competition is present only at nonzero temperatures, and is merely due to topological constraints of the ribbon. Another, more physical way of understanding this competition is to consider the interaction between two neighboring twisted regions. It is easy to see that twists of opposite sign meeting at an edge tend to unwind (annihilate) each other [17], while twists of the same sign are trapped when they meet; they do not annihilate each other and add up (see Fig. 3).

V. SIMULATION

An intriguing feature of the behavior of this model is that, although the ground state $(T=0)$ configuration of the system is a flat ribbon, and supports no twists, upon raising the temperature, a twisted structure with short-range *twist* order develops. We have confirmed this by performing extensive molecular dynamics (MD)/Monte Carlo (MC) simulations of double-stranded semiflexible polymers. A bead-spring model with bending and stretching energies was used. We combined a velocity Verlet MD algorithm coupled to a heat bath with an off-lattice pivot MC algorithm. The MD was useful for equilibrating the shorter length scales and MC for the long length scales.

We used a triangular lattice to discretize the ribbon (see Fig. 4). The position of the ith bead is $\mathbf{r}_i$ and we assume all the beads have mass m. The two chains making up the double strands join the odd $(\{1,3,5,\ldots,799\})$ and even $(\{2,4,6,\ldots,800\})$ beads together. The potential energy is given by

$$\frac{U[\{\mathbf{r}_i\}]}{k_B T} = \sum_{i=1}^{N-2} k_s[(\mathbf{r}_{i+1}-\mathbf{r}_i)^2-\ell_0^2] + k_s[(\mathbf{r}_{i+2}-\mathbf{r}_i)^2-\ell_0^2] - k_b\cos\theta_i, \tag{19}$$

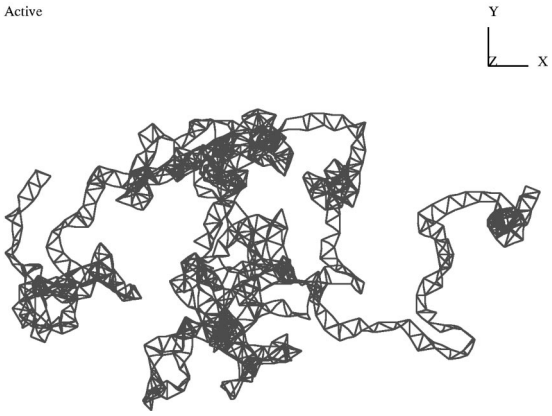

FIG. 5. Typical conformations from MD/MC simulations of a ribbon made up of two chains of 400 monomers above $T_\times$, $k_b=1$.

where

$$\cos\theta_i = (\mathbf{r}_{i+2}-\mathbf{r}_i)\cdot(\mathbf{r}_i-\mathbf{r}_{i-2}).$$

We have a bending constant k_b only for the springs joining beads on the same chain and a stretching constant k_s for every spring. We also have a short-range repulsion between nearest neighbor beads. The MD simulation is performed by integrating a Langevin equation for every bead,

$$m\frac{d^2\mathbf{r}_i}{dt^2} + \Gamma\frac{d\mathbf{r}_i}{dt} = -\boldsymbol{\nabla}_{r_i}U + f_i, \tag{20}$$

where f_i is a random number chosen from a range set by T representing the heat bath. The simulations were performed at $k_B T=1$. We are in the dissipative regime so we can ignore the inertial term. The friction term is set to $\Gamma=0.7$ and the noise is chosen so as to satisfy the fluctuation dissipation theorem. The equilibrium bond length was set to $\ell_0=1.6$. The simulations were done with $k_s=1000$.

We performed in general 10^6 integration time steps followed by 10^4 attempted pivot moves. A pivot move is an attempt to rotate a portion of the chain by a small random angle around a randomly chosen bead. The MC part is done with the usual Metropolis algorithm accepting pivot moves with a probability $\exp(-\Delta U/k_B T)$. This mixed MD/MC procedure was repeated 10^3 times until the configurations were equilibrated. Equilibration was checked by starting from crumpled chains and fully extended chains and verifying that the same values for radius of gyration and correlation functions were obtained. We simulated double-stranded ribbon chains of 2×400 monomers. The simulations were performed on a Cray T3D with 128 processors allowing us to simulate 128 chains in parallel.

Typical equilibrated polymer configurations, shown here in Figs. 5–7, suggest that at low temperatures the polymer can be viewed as a collection of long, twisted (straight) rods that are connected by short, highly curved sections of chain which we call ''kinks,'' as opposed to a smooth wormlike conformation. This structure melts at higher temperatures.

We plot the $\langle\mathbf{b}(s)\cdot\mathbf{b}(0)\rangle$ correlation function from the simulation in Fig. 8. For $T>T_\times$ we obtain simple exponen-

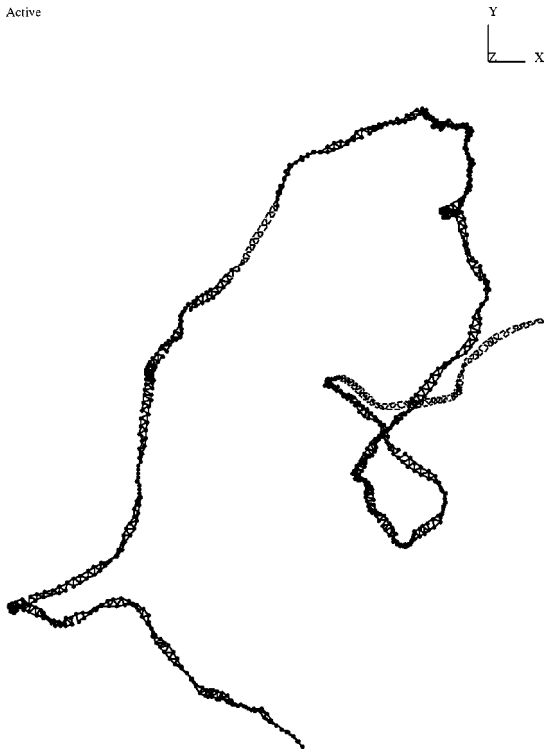

FIG. 6. Typical conformations from MD/MC simulations of a ribbon made up of two chains of 400 monomers near $T_\times$, $k_b=10$.

tial decay but for $T<T_\times$ we see an oscillation in the correlation function in agreement with Eq. (13).

We plot the $\langle \mathbf{t}(s)\cdot\mathbf{t}(0)\rangle$ correlation function from the simulation in Fig. 9. We see the signature exponential decay of the correlation function of wormlike chains from which we can estimate the effective persistence length. The estimated persistence lengths are $L_p=2.99\pm0.01,25.0\pm0.005,179.0\pm0.001$, respectively.

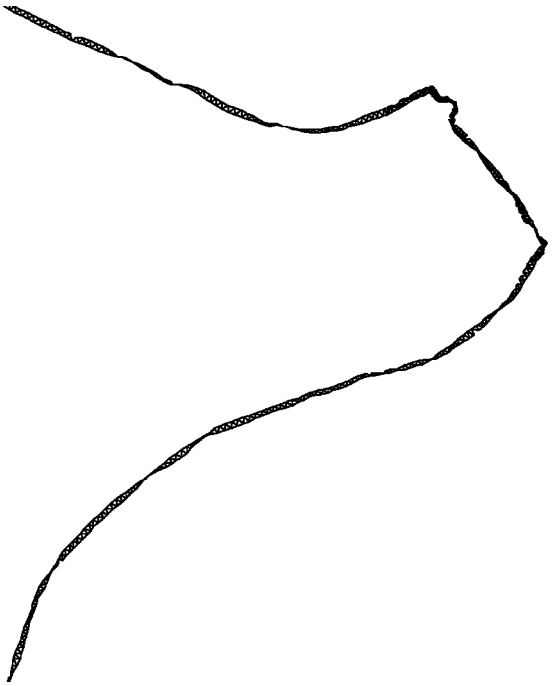

FIG. 7. Typical conformations from MD/MC simulations of a ribbon made up of two chains of 400 monomers below $T_\times$, $k_b=100$.

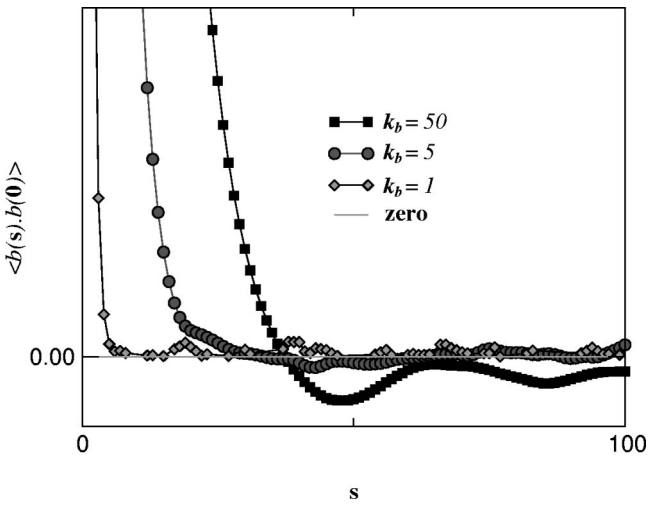

FIG. 8. The $\langle \mathbf{b}(s)\cdot\mathbf{b}(0)\rangle$ correlation function measured in the simulations for temperatures $k_b=1$, 5, and 50 corresponding to $b^2>c$, $b^2\approx c$, and $b^2<c$. The averages were done over $\sim10^4$ statistically independent samples. The error bars are the size of the symbols.

VI. KINK-ROD STRUCTURE

We show typical equilibrated conformations above, near, and below $T_\times$ in Figs. 5–7. The snapshots of the polymer configurations suggest that at low temperatures the polymer can be viewed as a collection of hard (straight) twisted rods that are connected by some kinks. This picture can be accounted for using a simple argument. We can model our system of two semiflexible polymers subject to the constraint of constant separation as a semiflexible ribbon, i.e., a semi-

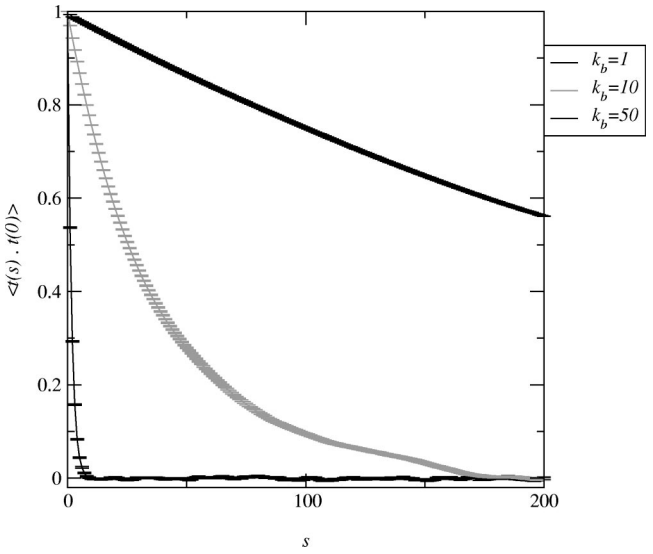

FIG. 9. The $\langle \mathbf{t}(s)\cdot\mathbf{t}(0)\rangle$ correlation function measured in the simulations for temperatures $k_b=1$, 10, and 50 corresponding to $b^2>c$, $b^2\approx c$, and $b^2<c$. The averages were done over $\sim10^4$ statistically independent samples. The error bars are the size of the symbols.

flexible linear object with anisotropic rigidities whose Hamiltonian reads

$$\mathcal{H}_{\rm ani}=\frac{1}{2}\int ds\sum_{i,j}\kappa_{ij}\left(\frac{d\mathbf{t}}{ds}\right)_i\left(\frac{d\mathbf{t}}{ds}\right)_j, \tag{21}$$

where $\kappa_{ij}=\kappa_\parallel b_i b_j+\kappa_\perp(\delta_{ij}-t_i t_j-b_i b_j)$ determines the rigidity anisotropy of the ribbon, corresponding to bending parallel or perpendicular to the bond-director field. The ribbon structure would require $\kappa_\parallel \gg \kappa_\perp$. [To be consistent with the hard constraint (see above) of constant separation of the polymers, we should take the limit of infinite $\kappa_\parallel$.] The partition function of a semiflexible ribbon in the $\kappa_\parallel\to\infty$ limit can be written as

$$\begin{aligned}\mathcal{Z}_{\rm rib}&=\lim_{\kappa_\parallel\to\infty}\int \mathcal{D}\mathbf{t}(s)\mathcal{D}\mathbf{b}(s)\exp\Bigg[-\frac{\kappa_\perp}{2k_BT}\int ds\left(\frac{d\mathbf{t}}{ds}\right)^2\\&\quad+\frac{\kappa_\parallel-\kappa_\perp}{2k_BT}\int ds\left(\frac{d\mathbf{t}}{ds}\cdot\mathbf{b}\right)^2+\mathcal{H}'[\mathbf{t},\mathbf{b}]\Bigg]\\&=\int \mathcal{D}\mathbf{t}(s)\mathcal{D}\mathbf{b}(s)\,\delta\left(\frac{d\mathbf{t}}{ds}\cdot\mathbf{b}\right)\exp\Bigg[-\frac{\kappa_\perp}{2k_BT}\int ds\left(\frac{d\mathbf{t}}{ds}\right)^2\\&\quad+\mathcal{H}'[\mathbf{t},\mathbf{b}]\Bigg],\end{aligned} \tag{22}$$

in which $\mathcal{H}'[\mathbf{t},\mathbf{b}]$ controls the dynamics of $\mathbf{b}$, and the functional δ function enforces the constraint

$$\frac{d\mathbf{t}(s)}{ds}\cdot\mathbf{b}(s)=0 \tag{23}$$

to hold exactly at every point of the ribbon. Recalling that $d\mathbf{t}/ds=H(s)\mathbf{n}$ from the Frenet-Seret equations [18], where $H(s)$ is the curvature at each point and $\mathbf{n}$ is the unit normal vector to the curve, we can write the constraint as

$$H(s)\mathbf{n}(s)\cdot\mathbf{b}(s)=0. \tag{24}$$

This constraint requires that at each point either $H(s)=0$, which corresponds to a straight (rodlike) segment that can be twisted, or $\mathbf{n}(s)\cdot\mathbf{b}(s)=0$, which corresponds to a curved (kinklike) region where the the bond director is locked into the perpendicular direction to the curve normal, i.e., the *binormal*.

We expect the (core) length of the kink regions to be very short at low temperatures, as observed in Fig. 7. We note that the conformational entropy of the chain is due to the degrees of freedom in the kink regions, whereas the twist entropy comes from the degrees of freedom in the rod segments. The average separation between neighboring kinks is of the order of the persistence length. The ribbon thus tends to keep the rod segments as long as possible to maximally explore the twist degrees of freedom, while it can recover the same conformational entropy as a wormlike chain from pivotal moves in the kink regions. This explains the kink-rod structure at low temperatures ($a\ll\ell_p$). As the temperature increases, the kinks get closer to each other, until at some temperature their average separation becomes comparable to their size ($\ell_p\sim a$), and the kink-rod pattern disappears.

This analysis can be understood in the context of the mean field ($\mathbf{b},\mathbf{t}$) model above. By observing that at low temperatures $\ell_{\rm BP}\ll\ell_{\rm TP}$, one can imagine that there are, roughly speaking, rodlike (straight) segments of length $\ell_{\rm TP}$, each supporting a number of shorter segments of length $\ell_{\rm BP}$ that are twisted but decorrelated with one other. One can see that $\ell_{\rm BP}$ is equal to the length scale λ at which the strands undergo conformational fluctuations of the order of their separation: $a^2=\langle r^2\rangle\equiv\int_{1/\lambda}dq/\ell_p q^4\simeq\lambda^3/\ell_p$. Hence, segments of length $\ell_{\rm BP}$ are straight (for $a\ll\ell_p$). However, fluctuations of order a are sufficient to wash out the memory of twist. The anticorrelation in fact comes from the frustration, as explained above.

As the temperature is raised, the number of twisted rods in each segment $N=\ell_{\rm TP}/\ell_{\rm BP}$ decreases very quickly, until it saturates to unity at $T=T_\times$. For higher temperatures the mechanism changes, and the bond correlations are cut off by the tangent fluctuations. Hence, the short-range twist order does not survive anymore. All the main features of the above picture have also been observed in the simulation.

A kink-rod structure similar to the one discussed here has indeed been observed in experiments done on actin filaments [19]. Actin is a charged polymer, and the mutual electrostatic repulsion of its different segments plays a major role in its structural stiffness. It is well known, however, that the introduction of *multivalent* counterions (ions of opposite charge that are necessary to neutralize the solution) can reduce the electrostatic repulsion, and even lead to attraction between like charged polymers, or different like charged segments of a same polymer [20]. In a recent experiment, Tang *et al.* [19] used fluorescence microscopy techniques to image *condensed* (or collapsed) actin bundles that are formed due to the presence of multivalent counterions. Snapshots of the bundles, showing their typical conformations, are shown in Fig. 10. A remarkable feature in the observation was the presence of sharp corners, which connect relatively straight segments of the actin bundles, as can be seen in Fig. 10. Tang *et al.* [19] observed that this feature is present only when the bundle is made up of two or more filaments of actin, and is absent when there is only a single filament in the condensate.

It is plausible to assume that the observed kink-rod structure can be accounted for by similar arguments to the one developed above. The only difference is the fact that the structure in the experimental case is a ring, as opposed to a chain with free ends. However, we do not expect this constraint to affect the argument, because the inherent competition between twist and bend degrees of freedom is local. Of course, more experimental efforts are needed to rule out other possible scenarios for the formation of the kinks, such as defects in the packing of more than one filament, sequence disorder, or metastable effects due to the dynamics of the collapse.

VII. MEAN FIELD THEORY: CONFINED CHAINS

In this section, we study the effect of confinement on double-stranded semiflexible polymers. We confine the double-stranded polymer in a $d_\perp$-dimensional subspace to a box of size R, while leaving it free in the remaining $d_\parallel=d-d_\perp$ dimensions.

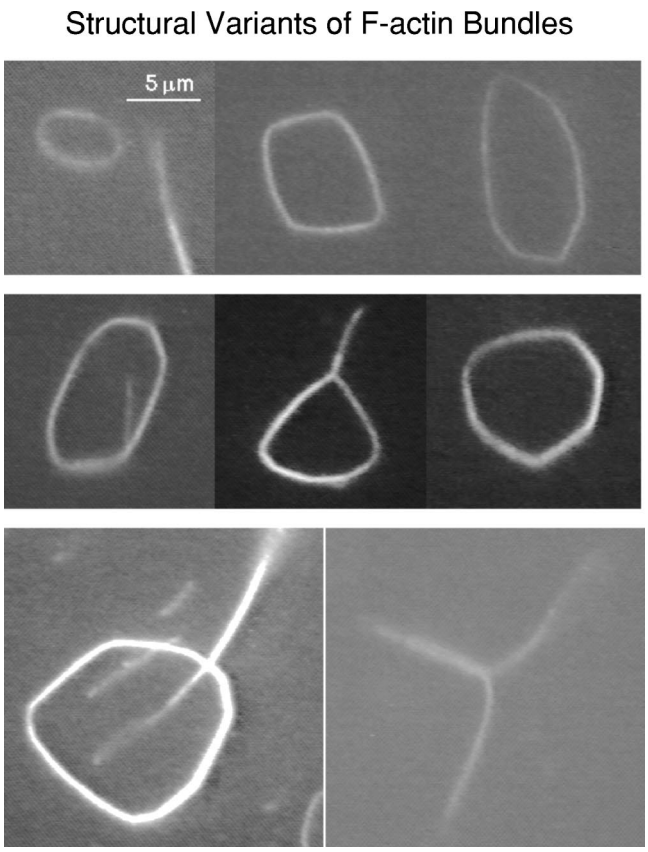

FIG. 10. Snapshots of condensed actin rings due to the presence of multivalent counterions, from the experiment by Tang *et al.* [19]. The kink-rod structure is manifest, in bundles with two or more filaments [19].

In terms of the tangent to the mid-curve $\mathbf{t}=d\mathbf{r}/ds$ and the bond director $\mathbf{b}$, the total Hamiltonian of the system can now be written as

$$\frac{\mathcal{H}_{\rm conf}}{k_BT}=\frac{\mathcal{H}+\mathcal{H}_m}{k_BT}+\frac{g}{\ell_p^3}\int ds\,\mathbf{r}_\perp^2\,, \tag{25}$$

where g is a dimensionless constant in addition to b, c, and e defined in Sec. III. The constants will be determined self-consistently by demanding that the relevant constraints hold on average: inextensibility of the individual strands, constant separation between the chains, the bond director being normal to the strands, and confinement of the polymer to a box of size R in $d_\perp$ dimensions $[\langle \mathbf{r}_\perp^2(s)\rangle = R^2]$. This final constraint is valid as long as the chain length is much larger than R. We obtain the following set of equations for b, c, e, and g:

$$\sqrt{c}\frac{a^2}{4\ell_p^2}+\sqrt{g}\frac{R^2}{\ell_p^2}+\frac{d_\parallel}{4\sqrt{2b}}=1,$$

$$c(b+\sqrt{c})=\frac{d^2\ell_p^4}{2a^4},$$

$$g(b+\sqrt{g})=\frac{d_\perp^2\ell_p^4}{32R^4},$$

TABLE I. The limiting behavior of the confined polymer: Asymptotic behavior of the solutions of Eq. (26).

			b	c	g
(1)	$\frac{R}{\ell_p}\ll 1$	$\frac{a}{\ell_p}\ll 1$	$\frac{d_\parallel^2}{32}$	$\left(\frac{d}{\sqrt{2}}\frac{\ell_p^2}{a^2}\right)^{4/3}$	$\left(\frac{d_\perp}{4\sqrt{2}}\frac{\ell_p^2}{R^2}\right)^{4/3}$
(2)	$\frac{R}{\ell_p}\gg 1$	$\frac{a}{\ell_p}\ll 1$	$\frac{d^2}{32}$	$\left(\frac{d}{\sqrt{2}}\frac{\ell_p^2}{a^2}\right)^{4/3}$	$\frac{d_\perp^2}{d^2}\frac{\ell_p^4}{R^4}$
(3)	$\frac{R}{\ell_p}\ll 1$	$\frac{a}{\ell_p}\gg 1$	$\frac{(d+d_\parallel)^2}{32}$	$\frac{16d^2}{(d+d_\parallel)^2}\frac{\ell_p^4}{a^4}$	$\left(\frac{d_\perp}{4\sqrt{2}}\frac{\ell_p^2}{R^2}\right)^{4/3}$
(4)	$\frac{R}{\ell_p}\gg 1$	$\frac{a}{\ell_p}\gg 1$	$\frac{d^2}{8}$	$\frac{4\ell_p^4}{a^4}$	$\frac{d_\perp^2}{4d^2}\frac{\ell_p^4}{R^4}$

$$e=0. \tag{26}$$

Although the above nonlinear set of equations is very difficult to solve, we can get the behavior of the solutions by looking at the asymptotics in the limiting cases, as summarized in Table I. The full solutions are in fact smooth interpolations between the asymptotics. We solved the equations numerically for the experimentally relevant case $d_\perp=1$ and $d=3$.

Having determined the constants self-consistently, we can calculate the correlation functions. For the tangent-tangent correlation in the parallel direction one obtains

$$\langle \mathbf{t}_\parallel(s)\cdot\mathbf{t}_\parallel(0)\rangle=\frac{d_\parallel}{4\sqrt{2b}}\exp\left(-\sqrt{2b}\,\frac{s}{\ell_p}\right), \tag{27}$$

whereas for the perpendicular direction one obtains

$$\begin{aligned}\langle \mathbf{t}_\perp(s)\cdot\mathbf{t}_\perp(0)\rangle=\frac{d_\perp}{8\sqrt{b^2-g}}\Bigg[&(b+\sqrt{b^2-g})^{1/2}\\ &\times\exp\left(-(b+\sqrt{b^2-g})^{1/2}\frac{s}{\ell_p}\right)\\ &-(b-\sqrt{b^2-g})^{1/2}\\ &\times\exp\left(-(b-\sqrt{b^2-g})^{1/2}\frac{s}{\ell_p}\right)\Bigg].\end{aligned} \tag{28}$$

Similarly, for the bond-director field it yields

$$\begin{aligned}\langle \mathbf{b}(s)\cdot\mathbf{b}(0)\rangle=\frac{d\ell_p^2}{2a^2\sqrt{b^2-c}}\Bigg(&\frac{\exp[-(b-\sqrt{b^2-c})^{1/2}(s/\ell_p)]}{(b-\sqrt{b^2-c})^{1/2}}\\ &-\frac{\exp[-(b+\sqrt{b^2-c})^{1/2}(s/\ell_p)]}{(b+\sqrt{b^2-c})^{1/2}}\Bigg),\end{aligned} \tag{29}$$

while the rest of the two-point functions (the cross terms) are zero. The parallel component of the tangent-director correlation function decays purely exponentially. However, the correlation function of the perpendicular component of the tangent-director field, as well as that of the bond-director field, develop a crossover from purely exponential decay for $b^2>g$ and $b^2>c$, to oscillatory decay for $b^2<g$ and $b^2<c$,

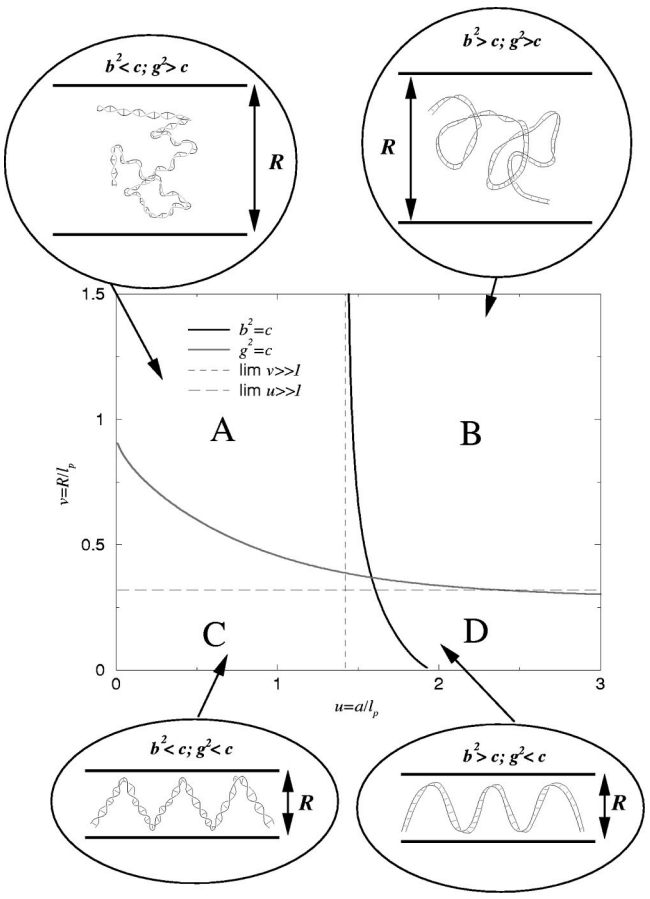

FIG. 11. The phase diagram as a function of $v=R/\ell_p$ and $u=a/\ell_p$ calculated numerically using Eq. (26). We work in three dimensions $d=3$ and with confinement in one direction $d_\perp=1$.

respectively. The phase diagram of the system in the space of dimensionless parameters R/ℓ_p and a/ℓ_p, is shown in Fig. 11. The boundaries between different regions are obtained from solutions of Eq. (26).

It is instructive to examine the perpendicular component of the tangent-director correlation function in the limiting case $b^2 \ll g$, which corresponds to $R/\ell_p \ll 1$ (see Table I). Using the asymptotic forms for b and g, one obtains

$$\langle \mathbf{t}_\perp(s)\cdot\mathbf{t}_\perp(0)\rangle = \left(\frac{d_\perp^2}{8\sqrt{2}}\frac{R^2}{\ell_p^2}\right)^{1/3} \times \exp\left[-\left(\frac{d_\perp}{16\ell_p R^2}\right)^{1/3} s\right] \times \sin\left[\left(\frac{d_\perp}{16\ell_p R^2}\right)^{1/3} s + \frac{\pi}{4}\right]. \tag{30}$$

The effects of confinement are best seen in this limiting expression. The persistence length of the polymer in the confined directions is reduced to $\ell_\perp \sim (\ell_p R^2)^{1/3}$. This ''deflection length'' [5] is in fact the length at which roughening of a semiflexible chain of bare persistence length ℓ_p becomes comparable to the confinement size (or separation of the confining walls) R: $R^2=\langle r_\perp^2\rangle = \int_{1/\ell_\perp} dq/\ell_p q^4$. In other words, the presence of the boundaries provides another competing mechanism to cut off tangent correlations in the directions of confinement. Moreover, the oscillatory form of the correlation function with a period $\lambda=\ell_\perp \sim (\ell_p R^2)^{1/3}$ implies a sinusoidal packing of the polymer in the confining cavity, where again the size of the oriented segments (the period of the oscillations) is set by the walls cutting off the roughness of the polymer. As seen in Sec. VI, a semiflexible ribbon develops a kink-rod structure at finite temperatures (due to the strong anisotropy in rigidity), in which rodlike segments (about a persistence length long) are connected by rather sharp kinks with a core size of the order of the diameter of the ribbon. If such a structure is restricted to a size less than the bare persistence length, new kinks have to be created at the confining walls to squeeze the ribbon into the available space. This therefore leads to the compact zigzag conformation of kinks and rods and the subsequent oscillatory tangent correlations.

It is straightforward to calculate the free energy of the system. We find

$$\frac{F}{k_BT} = \frac{F_0(b)}{k_BT} + \frac{L}{2\ell_p}\left((b+\sqrt{b^2-c})^{1/2} + (b-\sqrt{b^2-c})^{1/2} + (b+\sqrt{b^2-g})^{1/2} + (b-\sqrt{b^2-g})^{1/2}\right). \tag{31}$$

It is interesting to examine the limiting behavior of the free energy as a function of R. We obtain

$$\frac{F(R)}{k_BT} \simeq \frac{L}{2\ell_p} \times \begin{cases} (d_\perp/2)^{1/3}(\ell_p/R)^{2/3} & \text{for } R/\ell_p \ll 1 \\ (\alpha d_\perp/d^2)(\ell_p/R)^2 & \text{for } R/\ell_p \gg 1, \end{cases} \tag{32}$$

where α is a smoothly varying numerical coefficient ranging from $\alpha=4$ for $a/\ell_p \ll 1$ to $\alpha=1$ for $a/\ell_p \gg 1$. The free energy, interestingly, interpolates between the steric repulsion of non-self-avoiding flexible polymers confined to R [21], which has $1/R^2$ behavior, and the Helfrich undulation free energy of stiff polymers confined to R [5,22], which has $1/R^{2/3}$ behavior [23].

Using the above results, we now analyze some recent experiments by Ott *et al.* [24] who measure the persistence length of actin filaments confined between microscope slides. The separation of the slides was of the order of $R=1$ μm and they found a persistence length (assuming a two-dimensional wormlike chain) of $L_p^0=16.7$ μm. These results are in the regime addressed by our model. For very small but finite R the chain fluctuates between the two plates. From the analog of Eq. (30) calculated for single-stranded semiflexible polymers, we find $\langle t_\perp^2\rangle = (R/L_p^{(0)})^{2/3}/2$. Therefore one must include the fluctuations perpendicular to the confining plates in the calculation of the true persistence length. This implies that on average the polymer makes an angle θ given by $\sin\theta=\sqrt{\langle t_\perp^2\rangle}$ with the plates where $\theta<1$. One therefore has a corrected persistence length $L_p^{\text{true}} \approx L_p^{(0)}/\cos\theta = L_p^{(0)}/\sqrt{1-\langle t_\perp^2\rangle}$. We therefore estimate for those experiments a correction of approximately 4%, i.e., $L_p^{\text{true}}=17.4$ μm.

VIII. CONCLUSION

In conclusion, we have calculated the properties of a well-defined model of a double-stranded semiflexible polymer and shown nontrivial differences between the high, low, and zero temperature behavior. At high T we find normal wormlike

chain behavior and at low T we observe a kink-rod structure with short-range twist order while at $T=0$ we have a flat ribbon.

In the analytical approach, the only approximation we have made is the relaxing of local constraints to global ones. Using a *systematic* $1/d$ expansion (see the Appendix) we have shown that to calculate the two-point correlation functions this is a valid approximation, as higher order corrections only change the values of parameters but do not change the analytic form of the functions. Extensive MD/MC simulations confirm the analytical results.

We have also examined the effect of confinement on the behavior of semiflexible double-stranded polymers, and found four interesting regimes of the conformation and internal twist structure of these polymers, as summarized in Fig. 11: (A) Weak confinement and relatively short bonds lead to free wormlike chain conformations with short-ranged twist anticorrelations, (B) weak confinement and relatively long bonds give rise to free wormlike chain conformations and twist disorder, (C) strong confinement and relatively short bonds yield sinusoidal packing of the chains and short-ranged twist anticorrelations, and finally (D) strong confinement and relatively long bonds lead to sinusoidal packing of the chains and twist disorder.

There are a number of advantages evident in our approach. First, we introduce a microscopic model that remains true to the chemical structure of many biomolecules. Second, our *approximate* method of solving this model also lends itself to the analysis of the fluctuations in the system and to studying intermediate-scale behavior as well as the ground state (long-length-scale) properties. Finally, this method could be easily extended to describe multistranded objects. We expect that the effect of an intrinsic twist will change the ground state but will not change any of the conclusions of our description, although we expect it to make the effective persistence length much higher. We hope to address such questions in a subsequent publication.

ACKNOWLEDGMENTS

It is a great pleasure to acknowledge many stimulating discussions with A. Ajdari, R. Ejtehadi, R. Everaers, E. Frey, G. Grest, M. Kardar, K. Kremer, A. Maggs, and M. Pütz. The financial support of the Max-Planck-Gesellschaft and the Training and Mobility of Researchers program of the European Union is gratefully acknowledged. This research was supported in part by EU Grant No. FMBICT972699 and the National Science Foundation under Grant Nos. PHY94-07194 and DMR-98-05833.

APPENDIX: 1/*d* EXPANSION

To justify the mean field approximations used in Secs. III and VII above, we perform a systematic $1/d$ expansion that allows us to implement the constraints in a controlled way. Our approach is similar to the one successfully used by David and Guitter to study the crumpling transition of crystalline membranes [14]. For simplicity, we consider a more primitive model of an elastic ribbon with the Hamiltonian

$$\frac{\mathcal{H}_{\rm ribbon}}{k_BT}=\frac{A}{2}\int ds\left(\frac{d\mathbf{t}}{ds}\right)^2+\frac{C}{2}\int ds\left[\frac{d\mathbf{b}}{ds}-\mathbf{t}\left(\mathbf{t}\cdot\frac{d\mathbf{b}}{ds}\right)\right]^2, \tag{A1}$$

in which the tangent and the bond-director fields are subject to the following constraints: $\mathbf{t}^2=1$, $\mathbf{b}^2=1$, $\mathbf{t}\cdot\mathbf{b}=0$, and $\mathbf{b}\cdot(d\mathbf{t}/ds)=0$ [Eq. (23)]. A similar calculation with the more realistic (and more complicated) Hamiltonian of Eq. (3) will lead to essentially the same conclusions. The partition function of the ribbon can be calculated as

$$\mathcal{Z}=\int \mathcal{D}\mathbf{t}\mathcal{D}\mathbf{b}\mathcal{D}\lambda_1\mathcal{D}\lambda_2\mathcal{D}\lambda_3\mathcal{D}\lambda_4 e^{-S(\mathbf{t},\mathbf{b},\lambda_1,\lambda_2,\lambda_3,\lambda_4)}, \tag{A2}$$

with

$$S=\frac{A}{2}\int ds\left(\frac{d\mathbf{t}}{ds}\right)^2+\frac{C}{2}\int ds\left(\frac{d\mathbf{b}}{ds}\right)^2+i\int ds\left[\lambda_1(s)(\mathbf{t}^2-1)+\lambda_2(s)(\mathbf{b}^2-1)+\lambda_3(s)(\mathbf{t}\cdot\mathbf{b})+\lambda_4(s)\left(\mathbf{t}\cdot\frac{d\mathbf{b}}{ds}\right)\right], \tag{A3}$$

in which $\{\lambda_\alpha(s)\}$ are the ''stress'' (Lagrange multiplier) fields enforcing the constraints. The integrations over $\mathbf{t}$ and $\mathbf{b}$ are now Gaussian and can be performed to yield

$$S_{\rm eff}[\lambda_i]=\frac{d}{2}\ln\det\begin{bmatrix}-A\partial_s^2+2i\lambda_1 & i\lambda_3+i\lambda_4\partial_s\\ i\lambda_3-i\partial_s\lambda_4 & -C\partial_s^2+2i\lambda_2\end{bmatrix}-id\int ds(\lambda_1+\lambda_2). \tag{A4}$$

Note that we have rescaled A,C, and $\{\lambda_\alpha(s)\}$ by d. Extremizing the effective action corresponds to the saddle-point or mean field solution ($d=\infty$). The saddle-point equations yield $i\overline{\lambda_1}=1/(8A)$, $i\overline{\lambda_2}=/(8C)$, and $\overline{\lambda_3}=\overline{\lambda_4}=0$.

To proceed to the higher orders in $1/d$, we need to calculate the λ propagators defined as

$$\langle\lambda_\alpha(s)\lambda_\beta(s')\rangle\equiv\left.\frac{\delta^2S_{\rm eff}}{\delta\lambda_\alpha(s)\,\delta\lambda_\beta(s')}\right|^{-1}_{\text{saddle point}}. \tag{A5}$$

A straightforward calculation then leads to

$$\langle\tilde\lambda_1(q)\tilde\lambda_1(-q)\rangle=\frac{A}{8d}q^2+O(1), \tag{A6}$$

$$\langle\tilde\lambda_2(q)\tilde\lambda_2(-q)\rangle=\frac{C}{8d}q^2+O(1), \tag{A7}$$

$$\langle\tilde\lambda_3(q)\tilde\lambda_3(-q)\rangle=\frac{A}{2d}q^2+O(1), \tag{A8}$$

$$\langle\tilde\lambda_4(q)\tilde\lambda_4(-q)\rangle=\frac{A+C}{2d}q^2+O(1/q^2), \tag{A9}$$

$$\langle\tilde\lambda_3(q)\tilde\lambda_4(-q)\rangle=\frac{A}{2d}(-iq)+O(1/q), \tag{A10}$$

while all the others are zero. Note that we have kept only the large momentum limit, since we are interested in the local (short-distance) behavior of the Lagrange multipliers [14].

The above λ propagators, the correlators for the tangent and bond fields

$$\langle \tilde{t}_i(q)\tilde{t}_j(-q)\rangle = \frac{\delta_{ij}}{Aq^2+1/(4A)}, \tag{A11}$$

$$\langle \tilde{b}_i(q)\tilde{b}_j(-q)\rangle = \frac{\delta_{ij}}{Cq^2+1/(4C)}, \tag{A12}$$

and the three-point vertices

$$\langle \tilde{t}_i(q)\tilde{t}_j(q')\tilde{\lambda}_1(-q-q')\rangle = 2i\delta_{ij}, \tag{A13}$$

$$\langle \tilde{b}_i(q)\tilde{b}_j(q')\tilde{\lambda}_2(-q-q')\rangle = 2i\delta_{ij}, \tag{A14}$$

$$\langle \tilde{t}_i(q)\tilde{b}_j(q')\tilde{\lambda}_3(-q-q')\rangle = i\delta_{ij}, \tag{A15}$$

$$\langle \tilde{t}_i(q)\tilde{b}_j(q')\tilde{\lambda}_4(-q-q')\rangle = -q'\delta_{ij}, \tag{A16}$$

as read from Eq. (A3), could now be used to construct diagrammatic expansions. Examining the two-point correlation functions for **t** and **b**, we then find that the perturbative expansions are well behaved (not singular), and only correct the numerical values of the coupling constants by finite amounts at each order. We thus conclude that the mean field behavior corresponding to the saddle-point approximation is qualitatively valid.

[1] M. Dogterom and B. Yurke, Phys. Rev. Lett. **81**, 485 (1998); V.V. Rybenkov, C. Ullsperger, A.V. Vologodski, and N.R. Cozzarelli, Science **277**, 690 (1997); M.S.Z. Kellermeyer, S.B. Smith, H.K. Granzier, and C. Bustamente, *ibid.* **277**, 690 (1997); J. Käs, H. Strey, and E. Sackmann, Nature (London) **368**, 226 (1994).

[2] P. Cluzel, A. Lebrun, C. Heller, R. Lavery, J-L. Viovy, D. Chatenay, and F. Caron, Science **271**, 792 (1996); S.B. Smith, Y. Cui, and C. Bustamante, *ibid.* **271**, 795 (1996); T.R. Strick, J.-F. Allemand, D. Bensimon, A. Bensimon, and V. Croquette, *ibid.* **271**, 1835 (1996).

[3] J.F. Marko and E.D. Siggia, Macromolecules **27**, 981 (1994); J.F. Marko, Europhys. Lett. **38**, 183 (1997); R.D. Kamien, T.C. Lubensky, P. Nelson, and C.S. O'Hern, *ibid.* **38**, 237 (1997).

[4] O. Kratky and G. Porod, Recl. Trav. Chim. Pays-Bas. **68**, 1106 (1949).

[5] T. Burkhardt, J. Phys. A **30**, L167 (1997); T. Odijk, Macromolecules **19**, 2313 (1986); W. Helfrich and W. Harbich, Chem. Scr. **25**, 32 (1985); A.R. Khoklov and A.N. Semenov, Physica A **112**, 605 (1982).

[6] R. Everaers, R. Bundschuh, and K. Kremer, Europhys. Lett. **29**, 263 (1995).

[7] T.B. Liverpool, R. Golestanian, and K. Kremer, Phys. Rev. Lett. **80**, 405 (1998).

[8] We are not the first or only authors to work on ribbon polymers. Different approaches can be found in I. A. Nyrkova, A. N. Semenov, and J.-F. Joanny, J. Phys. (France) II **6**, 1411 (1996); **7**, 825 (1997); **7**, 847 (1997); and S. Kumar and J. Singh, J. Stat. Phys. **89**, 981 (1997). For interesting extensions of our approach see Z. Haijun, Z. Yang, and O.-Y. Zhong-can, Phys. Rev. Lett. **82**, 4560 (1999); e-print cond-mat/9901321.

[9] M.G. Bawendi and K.F. Freed, J. Chem. Phys. **83**, 2491 (1985).

[10] J.B. Lagowski, J. Noolandi, and B. Nickel, J. Chem. Phys. **95**, 1266 (1991).

[11] A.M. Gupta and S.F. Edwards, J. Chem. Phys. **98**, 1588 (1993).

[12] T.B. Liverpool and S.F. Edwards, J. Chem. Phys. **103**, 6716 (1995).

[13] B.-Y. Ha and D. Thirumalai, J. Chem. Phys. **103**, 9408 (1995).

[14] F. David and E. Guitter, Europhys. Lett. **5**, 709 (1988).

[15] R.M. Hornreich, R. Liebmann, H.G. Schuster, and W. Selke, Z. Phys. B: Condens. Matter **35**, 91 (1979).

[16] C.S. O'Hern, R.D. Kamien, T.C. Lubensky, and P. Nelson, Eur. Phys. J. D **1**, 95 (1998).

[17] Note that we have changed our sign convention from [7] in defining twists.

[18] B.A. Dubrovin, A.T. Fomenko, and S.P. Novikov, *Modern Geometry—Methods and Applications Part I: The Geometry of Surfaces, Transformation Groups and Fields* (GTM Springer-Verlag, New York, 1984).

[19] J.X. Tang, J.A. Käs, J.V. Shah, and P. A. Janmey (unpublished).

[20] See, for example, R. Golestanian, M. Kardar, and T.B. Liverpool, Phys. Rev. Lett. **82**, 4456 (1999), and references therein.

[21] P.G. de Gennes, *Scaling Concepts in Polymer Physics* (Cornell University Press, Ithaca, NY, 1970).

[22] W. Helfrich, Z. Naturforsch. A **33**, 305 (1978).

[23] In general, the entropic undulation free energy for a D-dimensional rigid manifold consists of contributions of a k_BT per contact, i.e., $F/L^D \sim k_BT/\xi^D$, where ξ, the Odijk deflection length, is the length scale at which the roughness of the rigid manifold causes the first contact: $R^2=\langle r_\perp^2\rangle \sim \int_{1/\xi} d^Dq/q^4 \sim \xi^{(4-D)}$. Replacing $\xi \sim R^{2/(4-D)}$ in the former expression yields a Helfrich undulation free energy that varies as $1/R^{2D/(4-D)}$. For rigid membranes ($D=2$) it gives $1/R^2$, whereas for stiff polymers ($D=1$) it gives $1/R^{2/3}$.

[24] A. Ott, M. Magnasco, A. Simon, and A. Libchaber, Phys. Rev. E **48**, 1642 (1993).